Proc. Estonian Acad. Sci. Phys. Math., 2003, **52**, 1, 30–42
https://doi.org/10.3176/phys.math.2003.1.04

Numerical simulation of waves and fronts in structured materials: a thermodynamic approach

Arkadi Berezovski[a], Jüri Engelbrecht[a], and Gérard A. Maugin[b]

[a] Department of Mechanics and Applied Mathematics, Institute of Cybernetics at Tallinn Technical University, Akadeemia tee 21, 12618 Tallinn, Estonia; Arkadi.Berezovski@cs.ioc.ee
[b] Laboratoire de Modélisation en Mécanique, UMR CNRS 7607, Université Pierre et Marie Curie (Paris 6), Case 162, 4 place Jussieu, 75252 Paris, cedex 05, France; gam@ccr.jussieu.fr

Received 8 October 2002

Abstract. A thermodynamically consistent form for the finite-volume numerical method for thermoelastic wave and front propagation is proposed. Such reformulation provides applicability of the Godunov-type numerical schemes based on averages of field variables to the description of nonequilibrium situations. The nonequilibrium description uses contact quantities instead of numerical fluxes. These quantities satisfy the thermodynamic consistency conditions which generalize the classical equilibrium conditions.

Key words: thermoelastic waves, phase transition fronts, finite-volume methods, thermodynamics of discrete systems.

1. INTRODUCTION

The propagation of waves and phase-transition fronts in thermoelastic solids is governed by the same field equations and equations of state (at least in the integral formulation). In linear thermoelastic media these equations can be reduced to the classical hyperbolic wave equation and to the parabolic heat equation. Problems arise in the propagation of thermoelastic waves and fronts in *inhomogeneous* media, such as laminated composites, functionally graded materials, mesoscopic granular media, and two-phase media, in other words, in media with a microstructure. From a practical point of view, these problems are reduced to the construction of relevant numerical algorithms. Possible rapid variations in the properties of considered materials and the simultaneous presence of compression and shear waves require at

least a second-order accuracy of the algorithms. Among successful methods with high accuracy and efficiency are the finite-volume schemes.

Finite-volume numerical methods (cf. [1,2]) are based on the integration of governing equations over a control volume which includes a grid element and a time step. This means that the resulting numerical scheme is expressed in terms of averaged field variables and averaged fluxes at boundaries of the grid elements. The equations of state determining the properties of a medium are also assumed to be valid for the averaged quantities. In fact, this is an assumption of the local equilibrium inside the grid element, where the local equilibrium state is determined by the averaged values of field variables.

To obtain a high-order accuracy, the stepwise distribution of the field variables is changed to a piecewise linear (or even nonlinear) distribution over the grid [3]. Such a reconstruction leads to a better approximation from the mathematical point of view and provides a high-order accuracy together with a certain procedure for suppressing spurious oscillations during computation. However, from the thermodynamic point of view, the reconstruction destroys the local equilibrium inside grid cells. This means that the equations of state are not valid in this case and even the meaning of thermodynamic variables (e.g. temperature and entropy) is questionable.

A possible solution of this problem is the description of the nonequilibrium states inside the grid elements in the framework of the thermodynamics of discrete systems [4]. The thermodynamic state space is extended in this theory by accounting for so-called *contact quantities* in addition to the usual local equilibrium variables. These quantities can be introduced into the finite-volume schemes in a natural way. The crucial hypothesis then is the connection between the excess energy and contact quantities which describe the nonequilibrium states of discrete systems. The next step is the extension of the classical equilibrium conditions to the nonequilibrium case. In the paper, the corresponding procedure is described on the simple example of a uniaxial motion of a slab.

The results of computations of a test problem for the propagation of thermoelastic waves in media with rapidly-varying properties (e.g. in functionally graded materials) are presented. The comparison of the results of computations with the experimental investigations of the impact-induced martensitic phase transformation is also given in the one-dimensional case.

2. SIMPLE EXAMPLE: UNIAXIAL MOTION OF A SLAB

In order to explain some of the key ideas with a minimal mathematical complexity, it is convenient to work in an essentially one-dimensional setting. Consider a slab, which in an unstressed reference configuration occupies the region $0 < x_1 < L$, $-\infty < x_2, x_3 < \infty$, and consider uniaxial motion of the form

$$u_i = u_i(x,t), \quad x = x_1, \tag{1}$$

where t is time, x_i are spatial coordinates, u_i are components of the displacement vector. In this case, we have only three nonvanishing components of the strain tensor

$$\varepsilon_{11} = \frac{\partial u_1}{\partial x}, \quad \varepsilon_{12} = \varepsilon_{21} = \frac{1}{2}\frac{\partial u_2}{\partial x}, \quad \varepsilon_{13} = \varepsilon_{31} = \frac{1}{2}\frac{\partial u_3}{\partial x}. \tag{2}$$

Particle velocities associated with (1) are

$$v_i(x,t) = \frac{\partial u_i}{\partial t}. \tag{3}$$

Without loss of generality, we can set $\varepsilon_{13} = 0, v_3 = 0$. Then we obtain uncoupled systems of equations for longitudinal and shear components which express the balance of linear momentum and the time derivative of the Duhamel–Neumann thermoelastic constitutive equation, respectively [5,6]:

$$\rho_0(\mathbf{x})\frac{\partial v_1}{\partial t} = \frac{\partial \sigma_{11}}{\partial x}, \qquad \frac{\partial \sigma_{11}}{\partial t} = (\lambda(\mathbf{x}) + 2\mu(\mathbf{x}))\frac{\partial v_1}{\partial x} + m(\mathbf{x})\frac{\partial \theta}{\partial t}, \tag{4}$$

and

$$\rho_0(\mathbf{x})\frac{\partial v_2}{\partial t} = \frac{\partial \sigma_{12}}{\partial x}, \qquad \frac{\partial \sigma_{12}}{\partial t} = \mu(\mathbf{x})\frac{\partial v_2}{\partial x}, \tag{5}$$

which are complemented by the heat conduction equation

$$C(\mathbf{x})\frac{\partial \theta}{\partial t} = \frac{\partial}{\partial x}\left(k(\mathbf{x})\frac{\partial \theta}{\partial x}\right). \tag{6}$$

Here σ_{ij} is the Cauchy stress tensor, ρ_0 is the density, θ is temperature, and $C(\mathbf{x})$ is the heat capacity per unit volume for a fixed deformation. The dilatation coefficient α is related to the thermoelastic coefficient m, and the Lamé coefficients λ and μ by $m = -\alpha(3\lambda + 2\mu)$. The indicated explicit dependence on the point **x** means that the body is materially inhomogeneous in general. These systems of equations, (4) and (5), can be solved separately. For simplicity, we focus our attention on the system of equations (4) for longitudinal components in an isothermal situation.

2.1. Dynamic loading

In a dynamic problem we shall look for piecewise smooth velocity and stress fields $v_1(x,t),\ \sigma_{11}(x,t)$ for inhomogeneous thermoelastic materials, which obey the following initial and boundary conditions:

$$\sigma_{11}(x,0) = v_1(x,0) = 0, \qquad \text{for} \quad 0 < x < L, \tag{7}$$

$$v_1(0,t) = v_0(t), \quad \sigma_{11}(L,t) = 0, \quad \text{for} \quad t > 0, \tag{8}$$

and satisfy the field equations

$$\frac{\partial(\rho_0(x)v_1)}{\partial t} - \frac{\partial \sigma_{11}}{\partial x} = 0, \qquad \frac{\partial}{\partial t}\left(\frac{\sigma_{11}}{\lambda(x) + 2\mu(x)}\right) - \frac{\partial v_1}{\partial x} = 0. \tag{9}$$

The system of equations (9) is a system of conservation laws which is suitable for a numerical solution by a finite-volume scheme. We analyse the recently proposed wave-propagation algorithm [1,2].

3. WAVE-PROPAGATION ALGORITHM

The system of equations for one-dimensional elastic waves (5) can be represented in the conservative form

$$\frac{\partial q}{\partial t} + \frac{\partial f(q,x)}{\partial x} = 0, \tag{10}$$

where

$$q(x,t) = \begin{pmatrix} \rho_0(x)v(x,t) \\ \sigma(x,t)/(\lambda(x)+2\mu(x)) \end{pmatrix}, \qquad f(q,x) = \begin{pmatrix} -\sigma(x) \\ -v(x) \end{pmatrix}.$$

In the standard wave-propagation algorithm [1], a computational grid with interfaces $x_{n-1/2} = (n-1)/2\Delta x$, time levels $t_k = k\Delta t$, and cells $C_n = [x_{n-1/2}, x_{n+1/2}]$ are defined. For simplicity, the grid size Δx and time step Δt are assumed to be constant. Then the cell average

$$Q_i^n \approx \frac{1}{\Delta x}\int_{x_{i-1/2}}^{x_{i+1/2}} q(x,t_n)\,dx \tag{11}$$

is updated at each time step as follows

$$Q_i^{n+1} = Q_i^n - \frac{\Delta t}{\Delta x}\left(\mathcal{A}^+\Delta Q_{i-1/2} + \mathcal{A}^-\Delta Q_{i+1/2}\right), \tag{12}$$

where

$$\mathcal{A}^+\Delta Q_{i-1/2} = \sum_{p=1}^{m}(s_{i-1/2}^p)^+\mathcal{W}_{i-1/2}^p, \tag{13}$$

and

$$\mathcal{A}^-\Delta Q_{i+1/2} = \sum_{p=1}^{m}(s_{i+1/2}^p)^-\mathcal{W}_{i+1/2}^p. \tag{14}$$

Here $s^+ = \max(s,0)$, $s^- = \min(s,0)$, and $s_{i-1/2}^p$ are speeds of waves $\mathcal{W}_{i-1/2}^p$ obtained from the solution of the Riemann problem at $x_{i-1/2}$ which consists of Eq. (10) with piecewise constant initial data

$$q(x,0) = \begin{cases} Q_{i-1} & \text{if} \quad x < x_{i-1/2}, \\ Q_i & \text{if} \quad x > x_{i-1/2}. \end{cases} \tag{15}$$

The above-mentioned approach uses so-called *cell-edge* flux functions [7]. The main assumption here is the satisfaction of the Rankine–Hugoniot conditions at $x_{i-1/2}$

$$Q_i - Q_{i-1} = \sum_{p=1}^{m}\mathcal{W}_{i-1/2}^p. \tag{16}$$

An alternative approach is to assume that a distinct flux function $f_{i-1/2}(q)$ is associated with each cell interface $x_{i-1/2}$. In this case the flux functions are called *cell-centred* [7]. When cell-centred flux functions are used, a generalized Riemann problem at cell interface $x_{i-1/2}$ takes place. It consists of the equation (compare to (10))

$$\frac{\partial q}{\partial t} + \frac{\partial F_{i-1/2}(q,x)}{\partial x} = 0, \tag{17}$$

together with the initial data (15), where

$$F_{i-1/2}(q,x) = \begin{cases} f_{i-1}(q) & \text{if} \quad x < x_{i-1/2}, \\ f_i(q) & \text{if} \quad x > x_{i-1/2}. \end{cases} \tag{18}$$

The solution of the generalized Riemann problem is obtained by using the decomposition of the flux difference $f_i(Q_i) - f_{i-1}(Q_{i-1})$ instead of the decomposition (16):

$$f_i(Q_i) - f_{i-1}(Q_{i-1}) = \sum_{p=1}^{m} \mathcal{Z}^p_{i-1/2}, \tag{19}$$

where $\mathcal{Z}^p$ are called f-waves [7], as they are analogous to the waves $\mathcal{W}^p$ from (16). Since each $\mathcal{Z}^p_{i-1/2}$ corresponds to $s^p_{i-1/2}\mathcal{W}^p_{i-1/2}$, the expressions for fluctuations $\mathcal{A}^+\Delta Q_{i-1/2}$ and $\mathcal{A}^-\Delta Q_{i+1/2}$ (see (13)) are simply replaced by

$$\mathcal{A}^+\Delta Q_{i-1/2} = \sum_{p:s^p_{i-1/2}<0} \mathcal{Z}^p_{i-1/2}, \tag{20}$$

$$\mathcal{A}^-\Delta Q_{i+1/2} = \sum_{p:s^p_{i+1/2}>0} \mathcal{Z}^p_{i+1/2}. \tag{21}$$

As is shown in [7], the obtained algorithm is second-order accurate for smooth solutions.

3.1. Linear elastic waves in heterogeneous media

The Jacobian matrix for the system (5) is

$$f_q(q,x) = \begin{pmatrix} 0 & -1/\rho_0(x) \\ -\lambda(x) - 2\mu(x) & 0 \end{pmatrix}, \tag{22}$$

with eigenvalues $\pm c(x)$, where the sound speed is given by

$$c(x) = \sqrt{(\lambda(x) + 2\mu(x))/\rho_0(x)}. \tag{23}$$

The corresponding eigenvectors are

$$r^{(1)}(x) = \begin{pmatrix} 1 \\ Z(x) \end{pmatrix} \quad \text{for} \quad s^{(1)}(x) = -c(x), \tag{24}$$

and

$$r^{(2)}(x) = \begin{pmatrix} 1 \\ -Z(x) \end{pmatrix} \quad \text{for} \quad s^{(2)}(x) = c(x), \tag{25}$$

where $Z(x) = \rho_0(x)c(x)$ is the impedance. For the linear problem with variable coefficients, the Riemann solver is defined by choosing the wave speeds to be the sound speed in the appropriate cell [7]

$$s^{(1)}_{i-1/2} = -\sqrt{\frac{\lambda_{i-1} + 2\mu_{i-1}}{\rho_{i-1}}}, \quad s^{(2)}_{i-1/2} = \sqrt{\frac{\lambda_i + 2\mu_i}{\rho_i}}. \tag{26}$$

Then the waves $\mathcal{W}^{(1)}$ and $\mathcal{W}^{(2)}$ must be of the form

$$\mathcal{W}^{(1)}_{i-1/2} = \alpha^{(1)}_{i-1/2} r^{(1)}_{i-1/2} = \alpha^{(1)}_{i-1/2} \begin{pmatrix} 1 \\ Z_{i-1} \end{pmatrix}, \tag{27}$$

$$\mathcal{W}^{(2)}_{i-1/2} = \alpha^{(2)}_{i-1/2} r^{(2)}_{i-1/2} = \alpha^{(2)}_{i-1/2} \begin{pmatrix} 1 \\ -Z_i \end{pmatrix}. \tag{28}$$

The values $\alpha^{(1)}_{i-1/2}$ and $\alpha^{(2)}_{i-1/2}$ are determined by the condition [7]

$$f_i(Q_i) - f_{i-1}(Q_{i-1}) = \sum_{p=1}^{2} \alpha^{(p)}_{i-1/2} s^{(p)}_{i-1/2} r^{(p)}_{i-1/2}. \tag{29}$$

This leads to the following characteristic property of the algorithm

$$\mathcal{A}^+ \Delta Q_{i-1/2} + \mathcal{A}^- \Delta Q_{i-1/2} = f_i(Q_i) - f_{i-1}(Q_{i-1}). \tag{30}$$

As noted above, these modifications may be thermodynamically inconsistent. Therefore, what we need is to reformulate this well-developed method in a consistent form for nonequilibrium situations.

4. THERMODYNAMIC REPRESENTATION

4.1. Discrete systems

It is salient to remind the reader of the notion of *discrete systems* in thermodynamics ([4]). In such thermodynamics, the thermodynamic state space is extended by means of so-called *contact quantities* in order to describe

nonequilibrium states. In this perspective a discrete system is a domain G of $\mathbf{R}^3$ that is separated from its environment G^* by a contact surface ∂G. The interaction between G and G^* is described by *contact quantities*. In a Schottky system *per se*, this interaction consists of heat, work, and mass exchanges. For instance, considering the rate of heat exchange $\dot{Q}$, the so-called *contact temperature*, Θ, is defined by the following inequality:

$$\dot{Q}\left(\frac{1}{\Theta}-\frac{1}{T^*}\right)\geq 0 \tag{31}$$

for vanishing work and mass exchange rates. Here T^* is the thermostatic temperature of the equilibrium environment. From (31) it follows that $\dot{Q}$ and the bracket have always the same sign. If we now suppose that there exists exactly one equilibrium environment for each arbitrary discrete system for which the net heat exchange between them vanishes, then the defining inequality (31) determines the contact temperature of the system as the thermostatic temperature T^* of the system's environment for which this net exchange vanishes. The *dynamic pressure*, π, and the *dynamic chemical potential*, ν, are defined analogously

$$\dot{V}\,(\pi-p^*)\geq 0, \qquad \dot{M}\,(\nu^*-\mu)\geq 0, \tag{32}$$

where $\dot{V}$ is the time rate of volume and $\dot{M}$ is the time rate of mass. The contact quantities so defined provide a complete thermodynamic description of nonequilibrium states of a separated discrete system. Note, however, that the values of the defined contact quantities differ from the values of usual bulk parameters of the case of local equilibrium.

In the required extension of the concepts of the thermodynamics of discrete systems to the *thermoelastic case*, in addition to Θ and the defining inequality (31), which governs heat exchange, we must define a *contact dynamic stress tensor* Σ_{ij} since the state space includes the deformation. Analogously to (31) that holds for $\dot{\varepsilon}_{ij}=0$, we have thus

$$\frac{\partial\varepsilon_{ij}}{\partial t}(\Sigma_{ij}-\sigma^*_{ij})\geq 0, \qquad (\dot{Q}=0). \tag{33}$$

Here σ^*_{ij} is the Cauchy stress tensor in the environment. Now it remains to establish the connection between the *bulk* quantities and the *contact* quantities.

4.2. Thermodynamic consistency conditions

Classical equilibrium conditions for any two single-component simple systems consist in the equality of temperatures, pressures, and chemical potentials in both systems

$$T^{(1)}=T^{(2)}, \quad p^{(1)}=p^{(2)}, \quad \mu^{(1)}=\mu^{(2)}. \tag{34}$$

Here temperature, T, pressure, p, and chemical potential, μ, are given by

$$\left(\frac{\partial U}{\partial S}\right)_{V,N} = T, \quad \left(\frac{\partial U}{\partial V}\right)_{S,N} = -p, \quad \left(\frac{\partial U}{\partial N}\right)_{S,V} = \mu, \tag{35}$$

where U is the internal energy, S is the entropy, V is volume, and N is mass of the system. In general, the internal energy of a discrete system that is not in equilibrium differs from the local equilibrium value by an excess energy:

$$U(S,V,N) - U_{\rm eq}(S_{\rm eq}, V_{\rm eq}, N_{\rm eq}) = U_{\rm ex}. \tag{36}$$

Assuming that the local equilibrium variables are defined as usual (see (35)), the contact quantities can be associated with the excess energy:

$$\left(\frac{\partial U_{\rm ex}}{\partial S}\right)_{V,N} = \Theta, \quad \left(\frac{\partial U_{\rm ex}}{\partial V}\right)_{S,N} = -\pi, \quad \left(\frac{\partial U_{\rm ex}}{\partial N}\right)_{S,V} = \nu. \tag{37}$$

Therefore, the equilibrium conditions (34) can be generalized to the nonequilibrium case as follows:

$$T^{(1)} + \Theta^{(1)} = T^{(2)} + \Theta^{(2)}, \quad p^{(1)} + \pi^{(1)} = p^{(2)} + \pi^{(2)}, \tag{38}$$

$$\mu^{(1)} + \nu^{(1)} = \mu^{(2)} + \nu^{(2)}. \tag{39}$$

In the considered elastic case, only the condition $(38)_2$ is relevant. It should be applied in a tensorial form

$$\sigma_{ij}^{(1)} + \Sigma_{ij}^{(1)} = \sigma_{ij}^{(2)} + \Sigma_{ij}^{(2)}. \tag{40}$$

We will apply the consistency condition (40) to determine the values of the contact quantities.

4.3. Contact quantities

The finite-volume algorithm (12) can also be represented in terms of contact quantities [5,6]:

$$Q_i^{n+1} = Q_i^n - \frac{\Delta t}{\Delta x}\left(C_i^+(Q_i^n) - C_i^-(Q_i^n)\right), \tag{41}$$

where $C^{\pm}$ denote corresponding contact quantities,

$$C^{\pm}(Q_i) = \begin{pmatrix} \Sigma^{\pm}(Q_i) \\ \mathcal{V}^{\pm}(Q_i) \end{pmatrix}. \tag{42}$$

Here $\mathcal{V}$ denotes, by duality, the contact deformation velocity.

The consistency condition (40) in the uniaxial case

$$(\Sigma_{11}^{+})_{i-1} - (\Sigma_{11}^{-})_i = (\sigma_{11})_i - (\sigma_{11})_{i-1}, \tag{43}$$

should be complemented by the kinematic condition [8] which can be rewritten in the small-strain approximation as follows:

$$(\mathcal{V}_1^{+})_{i-1} - (\mathcal{V}_1^{-})_i = (v_1)_i - (v_1)_{i-1}. \tag{44}$$

The relations (43) and (44) can be expressed in vectorial form as follows:

$$C_{i-1}^{+}(Q_{i-1}^{n}) - C_i^{-}(Q_i^{n}) = f_i(Q_i) - f_{i-1}(Q_{i-1}). \tag{45}$$

It is easy to see that the last expression is nothing else but the characteristic property (30) for the conservative wave-propagation algorithm.

Thus, the thermodynamic consistency conditions and kinematic conditions at the cell edge automatically lead to the conservative wave-propagation algorithm. From another point of view, this means that *the wave-propagation algorithm is thermodynamically consistent*.

In practice, we note that the contact velocities are connected with contact stresses by relations along characteristic lines of the system of equations (9)

$$(\mathcal{V}_1^{-})_i = -\frac{(\Sigma_{11}^{-})_i}{\rho_i c_i}, \qquad (\mathcal{V}_1^{+})_{i-1} = \frac{(\Sigma_{11}^{+})_{i-1}}{\rho_{i-1} c_{i-1}}. \tag{46}$$

Therefore, we have a linear system of equations for the determination of contact stresses

$$(\Sigma_{11}^{+})_{i-1} - (\Sigma_{11}^{-})_i = (\bar{\sigma}_{11})_i - (\bar{\sigma}_{11})_{i-1}, \tag{47}$$

$$\frac{(\Sigma_{11}^{+})_{i-1}}{\rho_{i-1} c_{i-1}} + \frac{(\Sigma_{11}^{-})_i}{\rho_i c_i} = (\bar{v}_1)_i - (\bar{v}_1)_{i-1}. \tag{48}$$

Solving the system of equations (47), (48), we obtain the values of contact quantities needed to update the state of each cell to the next time step within the finite-volume numerical scheme (41).

5. NUMERICAL RESULTS

First we consider the stress wave propagation in the one-dimensional setting. Our motivation is to draw parallels with a similar problem discussed by Cermelli and Pastrone [9] who have shown the possible decay of the wave amplitude by a layer where some microscopic damage has accumulated. Their model was based on the concept of internal variables (cf. also [10]). The microstructure is then described by a certain scalar field that depends on the density of the defect and affects the energy function. It results in a certain additional nonequilibrium stress accounted

for in governing equations [9]. In our calculation, a layer of functionally graded material is placed in the interval [300,700] within the dimensionless computational domain [0,1000] (see Fig. 1). The mechanical properties of the layer are given by a mixture of randomly embedded particles with a Gaussian distribution function (Fig. 1). The properties of the metal and ceramic are the following [11,12]: Young's modulus 199.5 GPa and 393 GPa, Poisson's ratio 0.3 and 0.25, and density $8900\ \mathrm{kg/m^3}$ and $3970\ \mathrm{kg/m^3}$, respectively. The results of calculations are shown in Fig. 2. Clearly, we get an expected decrease in the transmitted wave amplitude after interaction with the layer. It should be noted that a considerable decrease is observed only in the case of a significant difference in the properties of materials. In addition, due to the random distribution in the layer, the reflected wave shows up certain irregularities (small wiggles about the zero line) that can be used for detecting the properties of the layer. By comparing the results obtained by the formalism of internal variables [9] and straightforward calculations, one could determine the properties of the scalar field used to model internal variables.

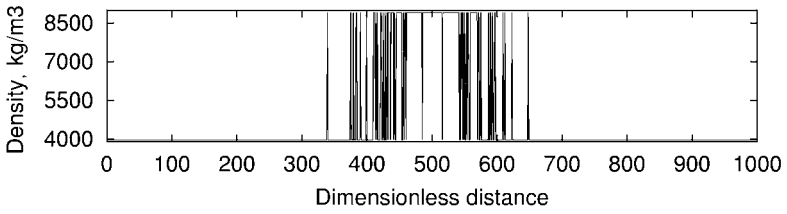

Fig. 1. Density distribution in a slab with inhomogeneous layer.

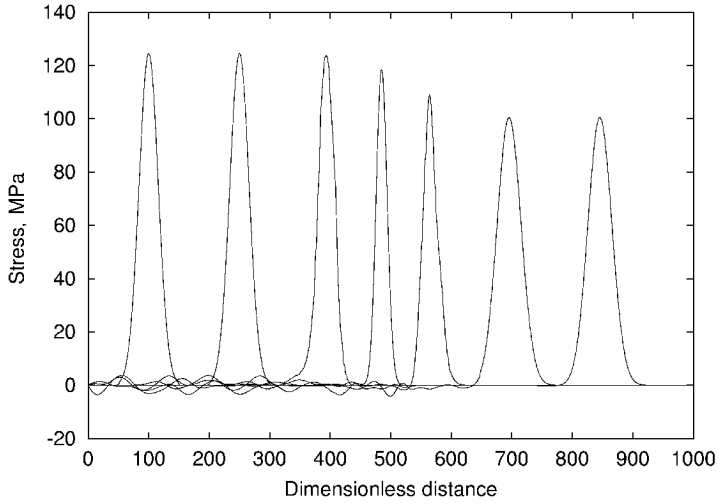

Fig. 2. Stress wave propagation inside a medium with inhomogeneous layer: stress profiles for consecutive time instants.

Now we will try to characterize the interaction of a shear stress wave with a phase boundary and to compare our simulations with available experimental data for a dynamical loading. To our knowledge, the only experimental investigation concerning impact-induced austenite-martensite phase transformations has been reported by Escobar and Clifton [13,14]. In their experiments, these authors used thin plate-like specimens of Cu-14.44Al-4.19Ni shape-memory alloy single crystal. One face of this austenitic specimen was subjected to an oblique impact loading, generating both shear and compression. The temperature changes during Escobar and Clifton's experiments are thought to be relatively unimportant. The measurements are taken in the central part of the rear face of the specimen. As Escobar and Clifton noted, measured velocity profiles provide several indications of the existence of a propagating phase boundary, in particular, a difference between the measured particle velocity and the transverse component of the projectile velocity. This velocity difference, in the absence of any evidence of plastic deformation, is indicative of a stress-induced phase transformation that propagates into the crystal from the impact face. To compare the results of our numerical simulation with the experimental data by Escobar and Clifton [13,14], we extract the properties of the austenite phase of the Cu-14.44Al-4.19Ni shape-memory alloy from their paper: the density $\rho = 7100\ \mathrm{kg/m^3}$, the elastic modulus $E = 120$ GPa, the shear wave velocity $c_s = 1187\,\mathrm{m/s}$, the dilatation coefficient $\alpha = 6.75 \times 10^{-6}\,1/\mathrm{K}$. For the martensitic phase we choose, respectively, $E =$ 60 GPa, $c_s = 1055\,\mathrm{m/s}$, with the same density and dilatation coefficient as above.

To compare the results of the modelling with the experimental data, the calculations of the particle velocity were performed for different impact velocities by means of the thermomechanical model of the phase transition front propagation [15,16] with a Courant number equal to 1. In the homogeneous case this gives the exact solution of the hyperbolic system of equations (5). The results of the comparison are given in Fig. 3, where the predictions of a simple model corresponding to a linear kinetic relation are also shown. It should be noted that the mobility coefficients in the linear model are calculated by means of the values of the driving force determined by the present numerical model and experimental data by Escobar and Clifton. Therefore, two different straight lines are based on the results of different experiments. As one can see, the linear models cannot approximate the experimental points related to remaining experiments. At the same time, the particle velocity computed by means of the present model is practically independent of the impact velocity, which has better correspondence with the available experimental data.

6. CONCLUSIONS

A thermodynamically consistent form for the finite-volume numerical method for thermoelastic wave and front propagation is proposed in the paper. Such a reformulation provides the applicability of the Godunov-type numerical schemes

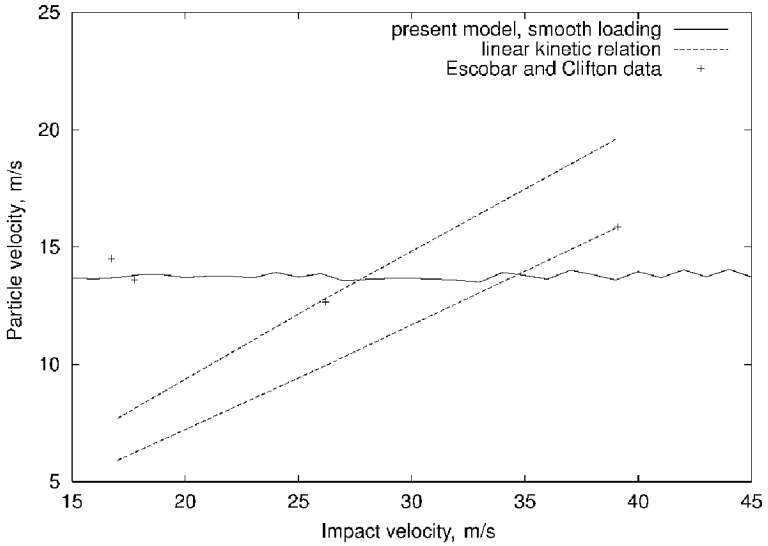

Fig. 3. Particle velocity versus impact velocity. Smooth loading.

based on averages of field variables to the description of nonequilibrium situations. The nonequilibrium description is fulfilled by using contact quantities instead of numerical fluxes. The contact quantities satisfy the thermodynamic consistency conditions which generalize the classical equilibrium conditions.

As is shown, numerical simulations performed by means of the modified finite-volume method capture both the theoretical predictions of decay of the wave amplitude by a damaged layer and the experimentally observed difference between tangential impact velocity and transversal particle velocity, which is indicative of the existence of phase transformation in a slab.

ACKNOWLEDGEMENTS

Support of the Estonian Science Foundation (grant No. 4504) (A.B.), European Science Foundation NATEMIS Programme (A.B. and J.E.), and European Network TMR. 98-0229 on “Phase transitions in crystalline substances” (G.A.M.) is gratefully acknowledged.

REFERENCES

1. LeVeque, R. J. Wave propagation algorithms for multidimensional hyperbolic systems. *J. Comp. Physics*, 1997, **131**, 327–353.
2. LeVeque, R. J. Balancing source terms and flux gradients in high-resolution Godunov methods: the quasi-steady wave-propagation algorithm. *J. Comp. Physics*, 1998, **148**, 346–365.

3. Barth, T. J. and Larson, M. G. *A posteriori* error estimates for higher order Godunov finite volume methods on unstructured meshes. In *Finite Volumes for Complex Applications III* (Herbin, R. and Kröner, D., eds.). Hermes, London, 2002, 41–63.
4. Muschik, W. Fundamentals of non-equilibrium thermodynamics. In *Non-Equilibrium Thermodynamics with Application to Solids* (Muschik, W., ed.). Springer, Wien, 1993, 1–63.
5. Berezovski, A., Engelbrecht, J. and Maugin, G. A. Thermoelastic wave propagation in inhomogeneous media. *Arch. Appl. Mech.*, 2000, **70**, 694–706.
6. Berezovski, A. and Maugin, G. A. Simulation of thermoelastic wave propagation by means of a composite wave-propagation algorithm. *J. Comp. Physics*, 2001, **168**, 249–264.
7. Bale, D. S., LeVeque, R. J., Mitran, S. and Rossmanith, J. A. A wave propagation method for conservation laws and balance laws with spatially varying flux functions. *SIAM J. Sci. Comp.*, **24**, 955–978.
8. Maugin, G. A. *Material Inhomogeneities in Elasticity*. Chapman and Hall, London, 1993.
9. Cermelli, P. and Pastrone, F. Exchange of energy between macro- and microstructure. In *Mesomechanics*, Vol. 1 (Sih, G. G., ed.). Tsinghua Univ. Press, Beijing, 2000, 201–208.
10. Engelbrecht, J., Cermelli, P. and Pastrone, F. Wave hierarchy in a microstructured solids. In *Geometry, Continua and Microstructure* (Maugin, G. A., ed.). Hermann, Paris, 1999, 99–111.
11. Cho, J. R. and Oden, J. T. Functionally graded material: a parametric study on thermal-stress characteristics using the Crank–Nicolson–Galerkin scheme. *Comput. Methods Appl. Mech. Engng.*, 2000, **188**, 17–38.
12. Cho, J. R. and Ha, D. Y. Averaging and finite-element discretization approaches in the numerical analysis of functionally graded materials. *Mat. Sci. Engng.*, 2001, **A302**, 187–196.
13. Escobar, J. C. and Clifton, R. J. On pressure-shear plate impact for studying the kinetics of stress-induced phase-transformations. *Mater. Sci. Engng.*, 1993, **A170**, 125–142.
14. Escobar, J. C. and Clifton, R. J. Pressure-shear impact-induced phase transformations in Cu-14.44Al-4.19Ni single crystals. In *Active Materials and Smart Structures*, *SPIE Proceedings*, 1995, **2427**, 186–197.
15. Berezovski, A., Engelbrecht, J. and Maugin, G. A. A thermodynamic approach to modeling of stress-induced phase-transition front propagation in solids. In *Mechanics of Martensitic Phase Transformation in Solids* (Sun, Q. P., ed.). Kluwer, Dordrecht, 2002, 19–26.
16. Berezovski, A. and Maugin, G. A. Thermodynamics of discrete systems and martensitic phase transition simulation. *Tech. Mechanik*, 2002, **22**, 118–131.

Lainete ja frontide numbriline modelleerimine struktureeritud materjalides: termodünaamiline lähenemine

Arkadi Berezovski, Jüri Engelbrecht ja Gérard A. Maugin

On esitatud termodünaamilisel kooskõlal põhinev lõplike mahtude numbriline meetod termoelastsete lainete ja frontide leviku kirjeldamiseks. Selline esitus lubab väljamuutujate keskmistel baseeruvaid Godunovi tüüpi numbrilisi skeeme rakendada mittetasakaaluliste pingeseisundite kirjeldamiseks. Mittetasakaaluline kirjeldus kasutab numbrilise voolu asemel kontaktsuurusi, mis rahuldavad termodünaamilise kooskõla tingimusi ja üldistavad klassikalisi tasakaalutingimusi.